



Cite this: *Phys. Chem. Chem. Phys.*,
2016, **18**, 28040

Benzoannelated aza-, oxa- and azaoxa[8]circulenes as promising blue organic emitters†

Gleb V. Baryshnikov,^{*ab} Rashid R. Valiev,^{acd} Nataliya N. Karaush,^a
Valentina A. Minaeva,^a Alexandr N. Sinelnikov,^c Stephan K. Pedersen,^e
Michael Pittelkow,^e Boris F. Minaev^{ab} and Hans Ågren^a

In the present work, we studied the synergetic effect of benzoannellation and NH/O-substitution for enhancing the absorption intensity in a series of novel designed benzoannelated aza- and oxa[8]circulenes. Semi-empirical estimations of the fluorescence rate constants allowed us to determine the most promising fluorophores among all the possible benzoannelated aza-, oxa- and mixed azaoxa[8]circulenes. Among them, *para*-dibenzoannelated [8]circulenes demonstrated the most intense light absorption and emission due to the prevailing role of the linear acene chromophore. Calculated ϕ_{fl} values are in complete agreement with experimental data for a number of already synthesized circulenes. Thus, we believe that the most promising circulenes designed in this study can demonstrate an intensive fluorescence in the case of their successful synthesis, which in turn could be extremely useful for the fabrication of future blue OLEDs. Special attention is devoted to the aromaticity features and peculiarities of the absorption spectra for the two highly-symmetrical (D_{4h} ground state symmetry) π -isoelectronic species as well as the so-called tetrabenzotetraaza[8]circulene and tetrabenzotetraoxa[8]circulene molecules. Both of them are characterized by rich electronic spectra, which can be assigned only by taking into account the vibronic coarse structure of the first electronic absorption band; the 0–1 and 0–2 transitions were found to be active in the absorption spectrum in complete agreement with experimental data obtained for both energy and intensity. The corresponding promotive vibrational modes have been determined and their vibronic activity estimated using the Franck–Condon approximation.

Received 6th May 2016,
Accepted 9th September 2016

DOI: 10.1039/c6cp03060b

www.rsc.org/pccp

1. Introduction

During the last few years hetero[8]circulenes (HC) have attracted a lot of attention^{1,2} because of their application in optoelectronic devices, such as organic light emitting diodes (OLEDs)³ and organic field-effect transistors (OFETs).^{4–6} Most HCs can also be represented as fragments of graphene-like materials, fullerenes and nanotubes.^{7–13} For example, the simplest tetraoxa[8]circulene has been recently predicted as the building block for novel porous one- and two dimensional materials, which are able to capture s- and d-block metal ions with high selectivity.^{10,11} Actually, these materials are new representatives of ion sieves and their high thermal and conformational stability has been proven by

phonon dispersion and frequency density of states calculations. The stability at finite-temperature has been additionally proved by *ab initio* molecular dynamics simulations.⁹

HC molecules are interesting objects for physical organic chemistry studies because of their unusual “bifacial” aromaticity, which strongly depends on the molecular structure and ionization impact. Generally all hetero[8]circulenes contain an internal eight-membered framework (*hub*-system) surrounded by an outer macrocycle (a so-called *rim*-system).^{14–18} Indeed, the balance between the diatropic and paratropic ring currents in the *rim*- and *hub*-systems determines the net aromatic, non-aromatic or anti-aromatic character of the hetero[8]circulenes and their charged forms.

Until recently, the number of synthesized HCs was limited to a few derivatives,^{19,20} but during the past decade novel tetraoxa[8]circulenes,³ octathia[8]circulene,²¹ tetrathiatetra-selena[8]circulene,⁶ azaoxa[8]circulenes,^{22–24} tetrathia[8]circulene and tetraselena[8]circulene^{25,26} have been synthesized and well characterized by both experimental and computational techniques.

The latest synthesized HC is tetrabenzotetraaza[8]circulene (TBTAC) obtained by Osuka *et al.* via a “fold-in” oxidative fusion reaction of 1,2-phenylene-bridged cyclic tetrapyrrole.²⁷ It is noteworthy that the pristine tetraaza[8]circulene (without outer

^a Division of Theoretical Chemistry and Biology, School of Biotechnology, KTH Royal Institute of Technology, 10691 Stockholm, Sweden. E-mail: gliabar@kth.se

^b Department of Chemistry and Nanomaterials Science, Bogdan Khmelitsky National University, Cherkasy, 18031, Ukraine

^c Tomsk State University, 36 Lenin Avenue, Tomsk, Russia

^d Tomsk Polytechnic University, 43a Lenin Avenue, Tomsk, Russia

^e Department of Chemistry, University of Copenhagen, Universitetsparken 5, DK-2100 Copenhagen Ø, Denmark

† Electronic supplementary information (ESI) available. See DOI: 10.1039/c6cp03060b

benzene fusions) was predicted and characterized theoretically one year before its successful synthesis.¹⁴ A lot of other “hypothetical” HCs have already been predicted computationally and their eventual synthesis remains a challenge for synthetic chemists.

The high symmetry of most of the hetero[8]circulene molecules causes fundamental restrictions in their electronic and vibrational spectra. Particularly, for the tetraoxa[8]circulene and tetraaza[8]circulene of the D_{4h} symmetry group the fluorescence from the first excited singlet (S_1) state is symmetry forbidden²⁸ and only a weak emission from the S_2 state of tetraoxa[8]circulene has been observed experimentally with the overall quantum yield being less than 0.1.³ The same low emission efficiency has been measured for the diazadioxo[8]circulene of the D_{2h} symmetry.²³ Incredibly, for octathia[8]circulene molecule with high D_{8h} symmetry the first allowed singlet–singlet transition takes place after tens of states without intensity.²⁹ All the synthesized HCs are extremely thermally stable compounds with a tight crystal packing, which provides good charge carrier motilities (both for holes and electrons).^{7,30,31} These are very useful properties for OLED applications, however, if we want to use the hetero[8]circulenes as luminescent materials we must activate their S_1 state, which is usually responsible for the fluorescence emission. In the present work we propose two possible concepts for improving the fluorescence of hetero[8]circulenes. The first concept concerns NH/O-substitution in the *rim*-system, which causes symmetry reduction; thus, the most strict symmetry restrictions disappear in the electronic spectra. The second concept is an additional benzoannulation of the benzenoid fragments in the *rim*-system. This also provides a molecular symmetry reduction and/or the S_1 state symmetry change, but additionally it enhances the light absorption/emission intensity due to the π -extending effect. The combination of these two concepts has allowed us to select the most promising fluorophores among all the possible benzoannulated aza-, oxa-, and mixed azaoxa[8]circulenes. We have also devoted special attention in this work to a pair of particular molecules, the fully-benzoannulated tetrabenzotetraoxa[8]circulene (TBTOC) and tetrabenzotetraaza[8]circulene (TBTAC) of the D_{4h} symmetry point group. In contrast to the pristine tetraoxa[8]circulene and tetraaza[8]circulene their tetrabenzotetraoxa[8]circulene derivatives have clearly visible vibronic-structured absorption and emission spectra with a fluorescence quantum yield (QY) of about 0.6 for TBTAC²⁷ and 0.16 for TBTOC as it is measured in the present work. Due to this experimental fact we have focused here in more detail on the next two points: (1) what is the effect of tetrabenzotetraoxa[8]circulene on the electronic structure and fluorescence of TBTAC and TBTOC, and (2) what is the origin of the vibronic progression in the absorption and fluorescence spectra of TBTAC and TBTOC. Each of these points will be discussed below in separate sections.

2. Computational details

A combination of benzoannulation and NH/O-substitution allows one to design 51 possible hetero[8]circulenes. Their molecular structures have been optimized at the B3LYP/6-311G(d,p)^{32–34} level of the density functional theory (DFT) with the control of

possible symmetry constraints using the Gaussian09 software package.³⁵ We have also calculated the vibrational frequencies and the corresponding IR intensities of the normal modes using the same method. All the vibrational frequencies have been found to be real indicating correct energy minima.

The energy levels of the S_1 and T_1 states have been calculated in the vertical approximation within the time-dependent density functional theory (TD-DFT) formalism³⁶ using the same B3LYP/6-311G(d,p) method. In order to examine the solvent effects on the energy and intensity of the S_0 – S_1 transitions we have used the polarizable continuum solvation model (PCM).³⁷

The vibronic structure of the TBTAC and TBTOC absorption spectra has been simulated within the Franck–Condon principle in the vacuum approximation using the optimized geometries, vibrational frequencies at the S_0 and S_1 states, and adiabatic electronic transition energy and transition dipole moment for the $S_0 \rightarrow S_1$ electronic transition of TBTAC and TBTOC. The profiles of the vibronic-structured absorption spectral curves have been constructed using the Gaussian distribution functions with the line half-width of 250 cm^{-1} . Due to the fact that TDDFT predicts the doubly-degenerate nature of the S_1 excited state for TBTAC and TBTOC we have additionally performed CASSCF(10,10) calculations with the next averaging over the S_0 – S_3 states and energy refinement using the XMC-QDPT³⁸ method including 30 states in the effective Hamiltonian. This is a new version of the CASPT2 approach.³⁹ All the XMC-QDPT2 calculations were carried out with the Firefly software.⁴⁰

The rate constants of the non-radiative electronic transitions (internal conversion and inter-system crossing channels) were estimated using the specially parameterized semi-empirical approximation. All the details of this method can be found in the literature.^{41,42} Here we describe briefly only the main points of the considered method. In this spectroscopically parameterized approximation the spin–orbit coupling (SOC) matrix elements and the non-adiabatic interactions between the singlet (S) and triplet (T) states were estimated using the intermediate neglected differential overlap level of theory with spectral parameters (INDO/S).^{41b} The excited S and T states energies were initially calculated using the TDDFT method (vertical approximation) and were used then in the semi-empirical calculations using perturbation theory as energy denominators.

The radiative rate constant (k_r , in s^{-1}) for the $S_1 \rightarrow S_0$ transition was calculated as follows:

$$k_r(S_1 \rightarrow S_0) = \frac{1}{1.5004} f_{S_1 \rightarrow S_0} \cdot (E_{S_1 \rightarrow S_0})^2,$$

where $E_{S_1 \rightarrow S_0}$ and $f_{S_1 \rightarrow S_0}$ are the excitation energy (in cm^{-1}) and oscillator strength for the $S_1 \rightarrow S_0$ transition, respectively.

The rate constant of the internal conversion (k_{IC}) between S_1 and S_0 states was estimated as follows:^{42d,e}

$$k_{IC} = \langle \varphi_{S_1} | \Omega | \varphi_{S_0} \rangle^2 \cdot Q_{S_1 \rightarrow S_0} \cdot E_{S_1 \rightarrow S_0}^{-2},$$

where φ_{S_1} and φ_{S_0} are the wavefunctions for the S_1 and S_0 states. The vibrational factor – $Q_{S_1 \rightarrow S_0}$ was estimated as follows:

$$Q_{S_1 \rightarrow S_0} = 10^{(14 - 0.2\lambda E_{S_1 \rightarrow S_0})},$$

where $\lambda = 10^{-3}$ cm for general case while $\lambda E_{S_1 \rightarrow S_0} = 1$ when $E_{S_1 \rightarrow S_0} < 10^3$ cm $^{-1}$. The matrix elements of non-adiabatic interaction were calculated using the formula:^{42,d,e}

$$\langle \varphi_{S_1} | \Omega | \varphi_{S_0} \rangle = \sqrt{N_{XH} \sum_x \left| \omega_{S_1 S_0}^x \right|^2},$$

where

$$\begin{aligned} \omega_{S_1 S_0}^x &= \sum_{ikl} A_{ik}^{S_1} A_{il}^{S_0} \sum_{\{o=x,y,z,s,H\}} (c_{ko} c_{lo})_x \\ &\quad - \sum_{ijk} A_{ik}^{S_1} A_{jk}^{S_0} \sum_{\{o=x,y,z,s,H\}} (c_{io} c_{jo})_x \\ &\quad + \sum_{ik} A_{ik}^{S_1} A_{ik}^{S_0} \sum_{\{o=x,y,z,s,H\}} (c_{ko}^2 - c_{io}^2)_x. \end{aligned}$$

Here, c_{io} – the expansion coefficients for the i -MO on the basis of the $2p_x$, $2p_y$, $2p_z$ atomic orbitals of the O, C and N atoms and the $1s$ -orbital of the H atoms. The $A_{ik}^{S_1}$ and $A_{ik}^{S_0}$ coefficients of configuration interaction (CI) expansion at INDO/S level of theory. N_{XH} is the total number of C-H, N-H and O-H bonds considering that only anharmonic vibrations of X-H bonds are assumed as promotive modes for non-adiabatic coupling interactions.

The rate constants of intersystem crossing (ISC) were estimated as follows:^{42fg}

$$k_{S_1 \rightarrow T_i} = 10^{10} \langle \varphi_{S_1} | H_{so} | \varphi_{T_i} \rangle^2 \cdot F_{0m},$$

where φ_{T_i} are the wavefunctions of the T_i states that are lower than the energy of the S_1 state. The integrals $\langle \varphi_{S_1} | H_{so} | \varphi_{T_i} \rangle$ are the SOC matrix element; they were calculated within the one-electron H_{so} operator approximation. The Franck-Condon factors were approximated using the formula:

$$F_{0m} = \sum_n \prod_{\nu} \frac{e^{-y} y^{n_{\nu}}}{n_{\nu}!},$$

where $n_{\nu} \approx \frac{E_{S_1 \rightarrow T_i}}{\omega_{\nu}}$. The Huang-Rhys factor y was assumed to be equal to 0.3 and only one average promotive mode $\omega_{\nu} \sim 1400$ cm $^{-1}$ was used.

The fluorescence quantum yield φ_f was calculated as follows:

$$\varphi_f = \frac{k_r}{k_r + k_{ic} + \sum_i k_{S_1 \rightarrow T_i}}.$$

In order to confirm the correctness of the semi-empirical calculations we have also calculated the k_r values and SOC matrix elements between S_1 and T_i states for the HCs with the

highest (>0.9) and lowest (<0.3) fluorescence quantum yields (predicted within INDO/S approximation) at the multi-configurational self-consistent field (MCSCF) level of theory. For this case we have used the one-electron Breit-Pauli H_{so} operator and XMC-QDPT2 calculated energies for the S_1 and T_i states as well as oscillator strengths for the S_0 - S_1 transitions.

Magnetically induced current density susceptibilities have been calculated using the GIMIC method.⁴³⁻⁴⁸ Nuclear magnetic resonance (NMR) shielding calculations that are needed for the GIMIC calculations of the current-density susceptibilities and the ring-current susceptibilities, which are also called current densities and ring-current strengths (in nA T $^{-1}$), were performed using the Turbomole software package.⁴⁹ The current density plots have been generated using the JMOL package.⁵⁰

The calculations were performed at the PDC supercomputer of the Royal Institute of Technology (Stockholm), at the CSC supercomputer of the Finnish IT Center for Science (Finland) and at the Tomsk State University (SKIF, Russia).

3. Results and discussion

3.1. Design strategy and structural features

The combination of two concepts – NH/O-substitution and benzoannulation – allows us to design all the possible hetero[8]-circulene molecules. Starting from the initial tetraaza[8]circulene **1** and using only NH/O-substitution we have received all the four possible mixed azaoxa[8]circulenes and also the totally substituted tetraoxa[8]circulene **6** (Fig. 1). This strategy has already been realized experimentally and the azacirculenes **4** and **5** were sufficiently synthesized and identified (with the additional side substituents).^{22,23} As a result, we have managed to increase the fluorescence QY up to 0.37 depending on the nature and size of the side substituents. Applying the second benzoannulation strategy for each of the six simplest circulenes we have designed 47 planar mixed HCs (Fig. 2) including all the possible isomers for the mono-, di- and triannulated species (for the detailed symmetry features see the ESI†). All of them are presented in Fig. 2 and can be classified by the two principles: (1) as the derivatives of HCs **1-6** (**1** → **47-51**; **2** → **7-15**; **3** → **25-35**; **4** → **36-41**; **5** → **16-24**; **6** → **42-46**) and (2) by the number of external benzene rings (monoannulated – **7, 10, 16, 19, 25, 29, 32, 36, 42, 47**; diannulated – **8, 11, 12, 14, 17, 20, 21, 23, 26, 30, 33, 35, 37-39, 43, 44, 48, 49**; triannulated – **9, 13, 18, 22, 27, 31, 34, 40, 45, 50**; tetraannulated – **15, 24, 28, 41, 46, 51**). Among the all HCs presented in Fig. 1 and 2 some species have been synthesized (**4, 5, 17, 42-45** by Pittelkow *et al.*,^{3,22,23}

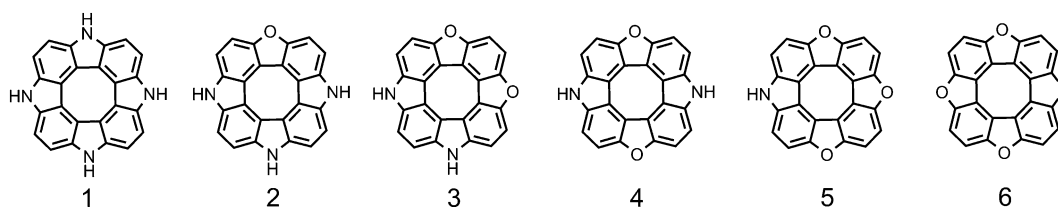


Fig. 1 The simplest hetero[8]circulenes constructed via the NH/O substitution principle in the rim-system.

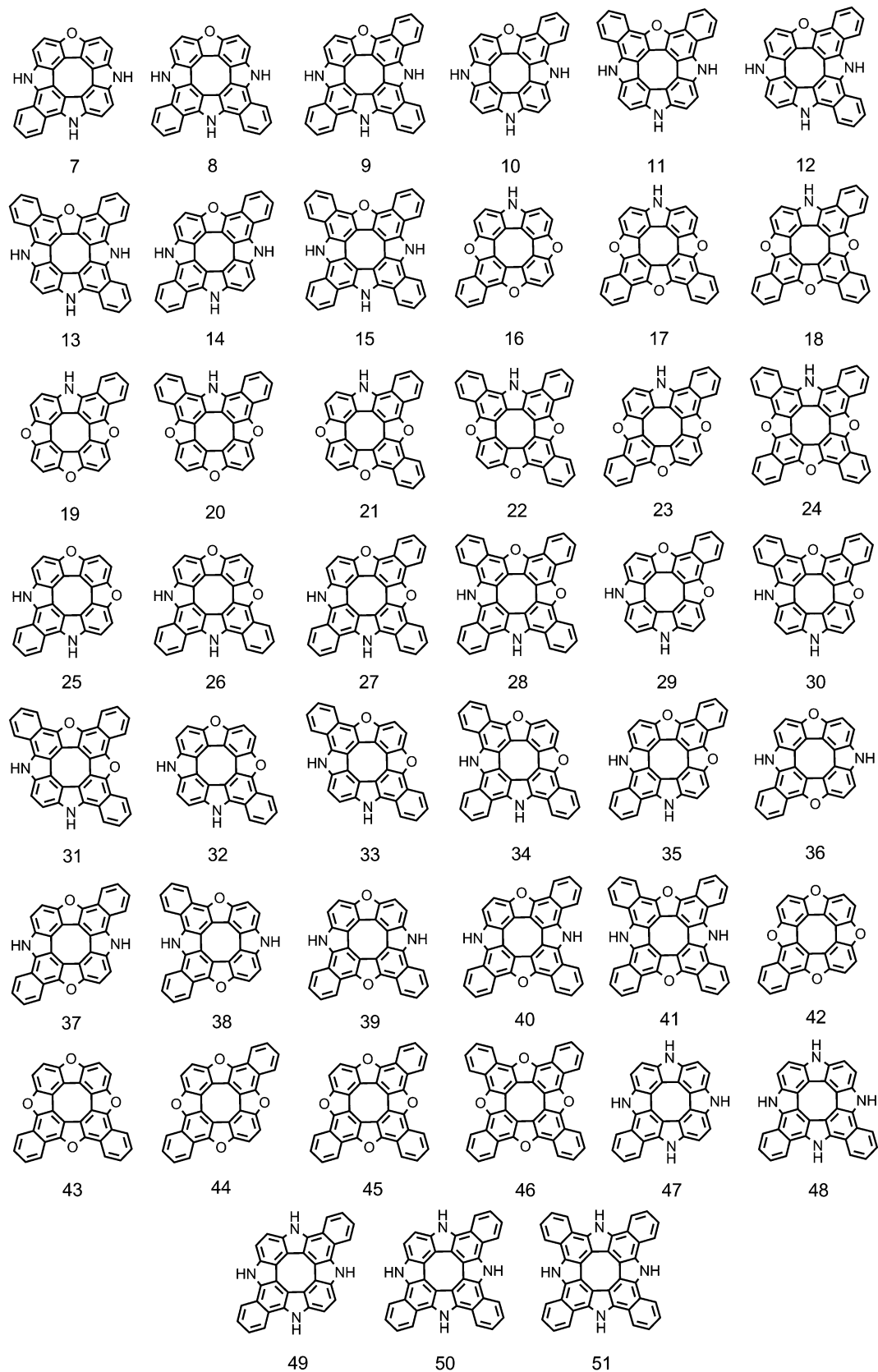


Fig. 2 All the possible hetero[8]circulenes constructed via the simultaneous NH/O substitution and benzoannulation of the initial HCs 1–6.

6 and 46 by Högberg^{19,20} and 51 by Osuka *et al.*²⁷ neglecting the side substituents), but the most of designed compounds were predicted here for the first time and these “hypothetical” molecules can be considered as the missing pieces of all the possible benzoannulated aza-, oxa- and azaoxa[8]circulenes. Notably, the proposed classification universal and can be applicable for other type of completely annulated tetraphenylenes with other heteroatoms in the *rim*-system (S/Se, PH/AsH or their combinations, for example) and other external fusion fragments (hetarenes or cycloalkanes, for example).

Among the simplest HCs 1–6 two diazadioxal[8]circulenes 3 and 4 represent the positional isomers. Our B3LYP/6-311(d,p) calculations predict that they are almost equivalent energetically and circulene 3 is only 0.46 kcal mol⁻¹ higher by the total energy value comparing with the already synthesized circulene 4.

The number of positional isomers was much higher in the case of the benzoannulated HCs (Fig. 2). However, all twelve groups of isomers possess very small energy differences inside the each group (less than 1 kcal mol⁻¹, Table 1). Particularly, among the twelfth group of isomers only one circulene, 26 was 1.03 kcal mol⁻¹ higher than the lowest isomeric HC 38. Moreover, in the case of isomers 43 and 44 it is impossible to determine the most stable form because of the extremely low energy difference between them (only 10⁻³ kcal mol⁻¹). Such energetic equivalence is due to the strong π -conjugation, which exists for all the designed species and the variations of molecular topology (*i.e.* changing of disposition between heteroatoms and external fusion fragments). This does not lead to significant perturbation of the HCs π -extended systems.

It is astounding that the (almost) energetically indistinguishable HC isomers are characterized by their clearly different photophysical properties, which are a consequence of the molecular topology and symmetry selection rules. This allows one to design HCs molecules with the required spectral features in a deliberated manner and, in particular, with

increased absorption and emission intensities required for OLED applications.

3.2. The absorption and emission features

A general feature of all the synthesized circulenes 5, 17, 6, 46, 42–45, 51, was the extremely small value of the Stokes shift (only a few nm) relative to the mirroring first band in the absorption and emission spectra. An exception was circulene 4, for which the emission occurs preliminary from the S₂ state with some admixture of the S₁ → S₀ component and therefore the mirror symmetry was absent in their absorption and fluorescence spectra.^{3,28} The small Stokes shift and mirror symmetry observed for most of the HC molecules indicates a small distortion in their molecular structure upon excitation into the S₁ state, which has also been indicated by previously published quantum-chemical calculations. It has been computationally shown⁵¹ that upon S₀ → S₁ excitation only the C–C bond alternation is changed in the central octatetraene core without any out-of-plane skeleton deformation and other significant distortions in the *rim*-system. Therefore, the oscillator strength for the vertical S₀ → S₁ transition must correlate with the corresponding value for the opposite S₁ → S₀ transition and also with the radiative rate constant (k_r) for the fluorescence emission. Really, as one can see from the Tables S2 and S3 (ESI[†]), the oscillator strength for the S₀ → S₁ transition and k_r values are generally in a linear relationship. Moreover, the theoretically estimated fluorescence quantum yields (ϕ_f) are also linearly dependent on the intensity of the S₀ → S₁ transition and k_r value in most cases. This is due to the fact that the non-radiative processes for most species are not competitive when compared with the radiative S₁ → S₀ emission. However, in some cases the relatively high oscillator strength values do not correspond to the high quantum yields because of the dominant role of the ISC processes. In order to confirm this statement we have summarized in the Table 2 the photophysical data obtained for the molecules with the estimated highest and lowest ϕ_f values as well as for molecules with known experimental ϕ_f values. As can be seen from Table 2 there is a good agreement between the theoretical (INDO/S) and experimental ϕ_f quantum yield values. Therefore, we believe that our ϕ_f estimations for the rest of the HCs (Table S3, ESI[†]) are reliable and correct. The mismatch between the experimental and theoretically estimated ϕ_f values for compounds 4–6 was due to the following reasons: (1) in the experimental conditions the real prototypes of compounds 4 and 5 are comprised of aliphatic substituents that cause symmetry reduction and therefore their real fluorescence quantum yield increases when compared with the highly symmetric ideal model for compounds 4 and 5 (Fig. 1) and (2) the non-zero quantum yield of compound 6 (TBTOC prototype) corresponds predominantly to emission from the S₂ state but in our calculations we have considered only the S₁ → S₀ transition probability (equal to zero within D_{4h} symmetry).

Considering Table 2 we have concluded that the main deactivation channels for the S₁ state of the HC molecules are the intersystem crossing and radiative transition to the ground state.

Table 1 The thirteen groups of isomers among the possible benzoannulated aza-, oxa- and azaoxal[8]circulenes and their corresponding energy differences (reported in the parentheses in kcal mol⁻¹)

Most stable isomer	High-lying isomers ^a
4	3 (+0.46)
10	7 (+0.45)
11	8 (+0.77), 12 (+0.38), 14 (+0.48)
13	9 (+0.32)
16	19 (+0.34)
17	20 (+0.54), 21 (+0.40), 23 (+0.38)
18	22 (+0.19)
36	25 (+0.85), 29 (+0.05), 32 (+0.45)
38	26 (+1.03), 30 (+0.35), 33 (+0.63), 35 (+0.81), 37 (+0.20), 39 (+0.19)
40	27 (+0.61), 31 (+0.13), 34 (+0.65)
41	28 (+0.68)
44	43 (+0.001)
48	49 (+0.17)

^a The data reported in the parentheses correspond to the B3LYP/6-311(d,p) energy differences relative to the most stable isomer accounting for zero-point energy corrections.

Table 2 The rate constants (in s^{-1}) and fluorescence quantum yield for the selected HCs

Molecule	Theory			Experiment ^a	
	k_r	k_{IC}	$\sum_i k_{S_1T_i}$	ϕ_{fl}	$\phi_{fl,exp.}^a$
4	0	3.4×10^5	1.1×10^8	0	0.1–0.2
5	1.8×10^4	3.0×10^5	7.1×10^5	0.02	0.3
6	0	2.5×10^5	0	0	0.09
15	1.2×10^8	2.7×10^5	6.1×10^5	0.99	—
17	4.8×10^6	3.9×10^3	4.7×10^5	0.91	0.91
18	1.5×10^8	1.6×10^5	5.5×10^6	0.96	—
23	1.6×10^8	2.5×10^5	7.8×10^6	0.95	—
25	7.4×10^7	4.1×10^5	1.5×10^5	0.99	—
33	1.5×10^8	3.1×10^5	1.6×10^6	0.99	—
36	9.9×10^7	6.4×10^5	5.5×10^8	0.16	—
42	6.5×10^6	4.5×10^6	1.2×10^5	0.58	0.55
43	1.5×10^7	1.1×10^7	6.9×10^5	0.57	0.51
44	1.6×10^8	1.9×10^7	3.1×10^6	0.88	0.83
45	2.2×10^6	1.9×10^6	6.1×10^6	0.27	0.36
47	6.3×10^6	5.8×10^5	3.6×10^7	0.14	—
46	1.4×10^8	4.4×10^3	1.5×10^5	0.99	0.16^b
49	1.5×10^8	7.5×10^5	1.6×10^6	0.98	—
51	9.7×10^7	4.5×10^5	2.50×10^6	0.97	0.55^b

^a Data taken from the literature.^{3,22,27} ^b The mismatch between the ϕ_{fl} and $\phi_{fl,exp.}$ was due to the strong aggregation of HCs **46** and **51** in the solvent medium.

The radiative $S_1 \rightarrow S_0$ channel dominates for molecules with high quantum yield ϕ_{fl} (>0.9), whereas ISC competes with the radiative $S_1 \rightarrow S_0$ process for the molecules with low ϕ_{fl} (<0.3). Therefore, the values of the SOC matrix elements and energy gaps between the S_1 and T_i states (i – number of triplets with energy less than S_1) play a key role in determination of the ϕ_{fl} values. In order to confirm this conclusion we have additionally performed *ab initio* XMC-QDPT2 calculations for the S_1 and T_i excited state energies and the SOC matrix elements between them for selected HCs (Table 3).

As can be seen from Table 3, the small energy gap and relatively large values of the SOC matrix elements between the

S_1 and T_2 states are the reasons for the low ϕ_{fl} values for **36**, **45** and **47**. In contrast, the $\langle \phi_{S_1} | H_{so} | \phi_{T_2} \rangle$ matrix elements are small for molecules with the highest ϕ_{fl} value (even equals zero for HCs **33** and **49**). It should be noted that the k_r values computed using the XMC-QDPT2 energies and oscillator strengths are one order of magnitude larger when compared with the k_r values calculated at the INDO/S level of theory. Nevertheless, the *ab initio* calculations generally confirm the main conclusions of the INDO/S results. Therefore, we can trust that compounds **15**, **18**, **23**, **25**, **33** and **49** should be excellent representatives of organic fluorophores.

Now, let us discuss the effects of the gradual substitution and annelation on the main spectroscopic characteristics of all the studied circulenes (excluding the initial circulenes **1–6**; Fig. 3).

As can be seen from Fig. 3, the averaged wavenumber for the $S_0 \rightarrow S_1$ transition monotonously decreases with the increase in the number of outer annelated benzene rings. At the same time, the calculated quantum yield and oscillator strength values increase upon benzoannelation. The gradual substitution of nitrogen atoms by oxygen does not provide a systematical effect on the wavelength of the $S_0 \rightarrow S_1$ absorption. However, the oscillator strength and quantum yield values exhibit a monotonous increase upon N/O substitution, reaching a maximum for the doubly-substituted *ortho*- and *para*-isomers (*o*-2B2N and *p*-2B2N species). We note that the *p*-2B2N HCs seem to be the most promising fluorophores (Table S2, ESI†) due to the *para*-effect, which implies a strong increase in the transition dipole moment component along the long molecular axis oriented across the opposite naphthalene fragments.

3.3. The absorption spectra of TBTAC and TBTOC

Among the whole manifold of the designed HCs, compounds **46** (TBTOC) and **51** (TBTAC) deserve special attention because of their unusual spectral features. Particularly, both of them demonstrate good fluorescence, in great contrast to compound **6**,

Table 3 A comparison of the INDO/S and XMC-QDPT2 calculated photophysical parameters for the selected molecules with the highest and lowest ϕ_{fl} values

Molecules	$S_1(f)$ (cm^{-1})	$k_r(INDO/S)$ (s^{-1})	$k_r(XMC-QDPT2)$ (s^{-1})	T_i	$\sum_i k_{S_1T_i}(INDO/S)$ (s^{-1})	$\langle \phi_{S_1} H_{so} \phi_{T_i} \rangle$ (cm^{-1})	ϕ_{fl}
15	25 627(0.2)	1.2×10^8	9.3×10^7	22 490	6.1×10^5	1.1 ($i = 1$)	0.99
				23 837		0.5 ($i = 2$)	
				25 485		0.2 ($i = 3$)	
18	26 636(0.5)	1.5×10^8	2.7×10^8	23 885	5.5×10^6	0.1 ($i = 1$)	0.96
				25 652		0.7 ($i = 2$)	
				21 487		0.1 ($i = 1$)	
23	25 868(0.7)	1.6×10^8	3.0×10^8	24 261	7.8×10^6	0.3 ($i = 2$)	0.95
				19 616		0.9 ($i = 1$)	
				21 561		0.1 ($i = 2$)	
25	23 769(0.3)	7.4×10^7	1.2×10^8	22 553	1.5×10^5	1.1 ($i = 1$)	0.99
				23 314		0.0 ($i = 2$)	
				21 637		0.1 ($i = 1$)	
33	25 218(0.2)	1.5×10^8	8.0×10^7	26 000	1.6×10^6	1.3 ($i = 2$)	0.99
				21 637		0.0 ($i = 2$)	
				26 000		1.6 ($i = 1$)	
36	26 312(0.2)	9.9×10^7	1.3×10^8	24 421	5.5×10^8	1.6 ($i = 1$)	0.16
				24 665		1.3 ($i = 2$)	
				24 421		0.0 ($i = 1$)	
45	25 230(0.3)	1.3×10^6	1.4×10^8	19 941	6.1×10^6	1.1 ($i = 2$)	0.27
				21 526		0.0 ($i = 1$)	
				21 526		1.4 ($i = 2$)	
47	22 633(0.1)	6.3×10^6	4.0×10^7	20 079	3.6×10^7	1.0 ($i = 1$)	0.14
				21 526		1.4 ($i = 2$)	
				21 526		0.0 ($i = 1$)	
49	22 351(0.2)	1.5×10^8	8.0×10^7	21 021	1.6×10^6	1.0 ($i = 1$)	0.98
				21 021		0.0 ($i = 2$)	
				21 021		0.0 ($i = 2$)	

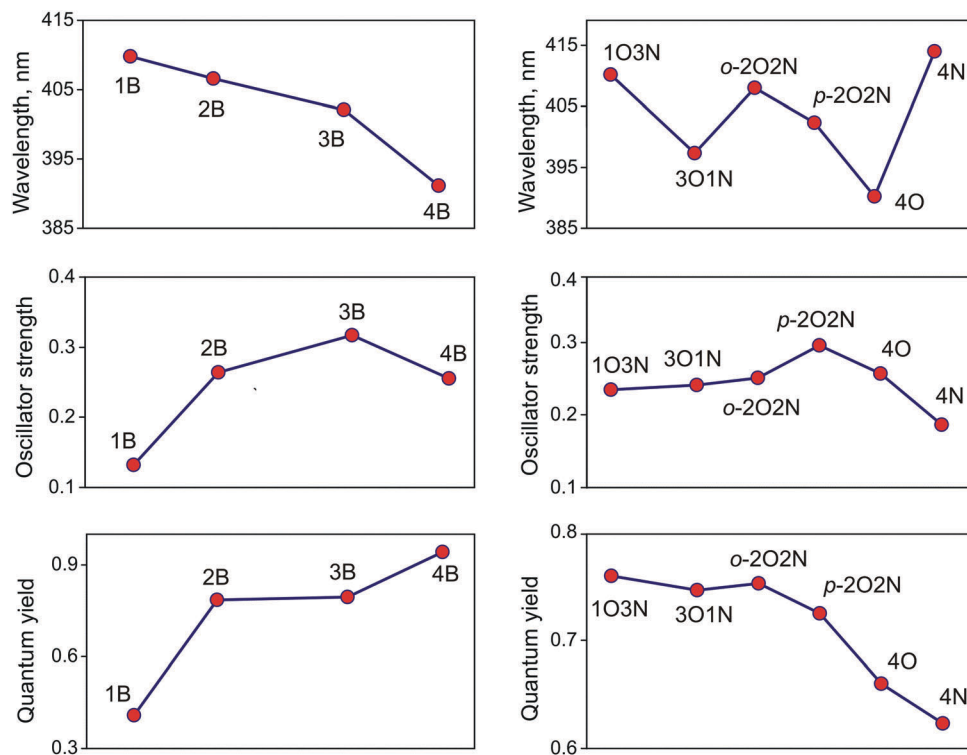


Fig. 3 The dependence of the averaged spectroscopic characteristics of HCs 7–51 on the gradual N/O-substitution (1O3N, 3O1N, *o*-2O2N, etc.) and benzoannellation (1B–4B).

which has no external benzene rings. The latter circulene **6** possesses the same D_{4h} molecular symmetry and for this compound the $S_0 \rightarrow S_1$ transition ($X^1A_{1g} \rightarrow 1^1A_{2g}$) is symmetry forbidden.²⁸ The same prohibition is also valid for the $S_0 \rightarrow S_1$ transition of the “hypothetical” tetraaza[8]circulene **1**. For this reason, the fluorescence for both **6** and **1** compounds was symmetry forbidden and only the doubly degenerated S_2 state of the 1E_u symmetry was formally allowed for light emission, providing a very weak fluorescence ($\varphi_f = 0.09$ for HC **6**). Surprisingly, the TBTOC species with the same D_{4h} symmetry group has a well-resolved intense fluorescence ($\varphi_f = 0.55$ in THF), which was obviously affected by the tetrabenzoannellation. From our measurements, the TBTOC compound demonstrates a quite moderate fluorescence quantum yield ($\varphi_f = 0.16$ in THF), which was explained by the strong stacking aggregation of the TBTOC molecules. However, in both cases we suggest that the four-times fusion of the *rim*-system with benzene fragments changes significantly the dispositions of the frontier molecular orbital energy levels and therefore, the symmetry allowed 1E_u state becomes lowest-lying singlet excited state level for the TBTOC and TBTOC molecules, providing the well-resolved fluorescence. Really, the tetrabenzoannellation of the initial tetraaza[8]circulene **1** (TAC) and tetraoxa[8]circulene **6** (TOC) causes the down-shift of their HOMO orbitals, while the next HOMO–1 and HOMO–2 orbitals of e_g symmetry provide an up-shift (Fig. 4). As a result, the first “dark” singlet excited state of circulenes **1** and **6** ($^1A_{1g}$ and $^1A_{2g}$, respectively) become the higher state for the TBTOC and TBTOC species than the lowest

lying doubly degenerate S_1 state of 1E_u symmetry (Table 4), which was responsible for the observable fluorescence of TBTOC and TBTOC. Notably, the MOs energies for the aza[8]circulenes **1** and **51** were significantly higher than the corresponding levels observed for oxa[8]circulenes **6** and **46** due to the donating effect of the NH groups. Therefore, the ionization potentials and electron affinities of the aza[8]circulenes are significantly lower than the corresponding values observed for the oxa[8]circulenes and it is the general trend for other related circulenes; the donating/accepting properties of the heteroatom in the *rim*-system determine the values of the ionization potentials and electron affinities of the whole manifold of HCs.

In order to prove our TDDFT-based assignment for the S_1 state for HCs **46** and **51** we have additionally performed XMC-QDPT2/6-311(d,p) calculations at a high *ab initio* level. We have observed a complete agreement between the TDDFT and XMC-QDPT2 methodologies relative to the double degeneracy of the S_1 state, its 1E_u symmetry and orbital assignment. The shapes of the molecular orbitals calculated using the XMC-QDPT2/6-311(d,p) method (see ESI†) are the same as the analogous MOs presented in Fig. 4. As can be seen from Table 4, the XMC-QDPT2/6-311(d,p) calculations provide a better agreement with the experimental results relative to the energy of the S_1 state when compared with the vertical TDDFT approximation. It was also clear that the adiabatic approximation (the 0–0 transition) definitely improves the agreement with the experimental band maximum obtained for **46** and **51**. It is notable that all the methods well reproduce the tendency that $E_{S_1}(\mathbf{46}) > E_{S_1}(\mathbf{51})$ and

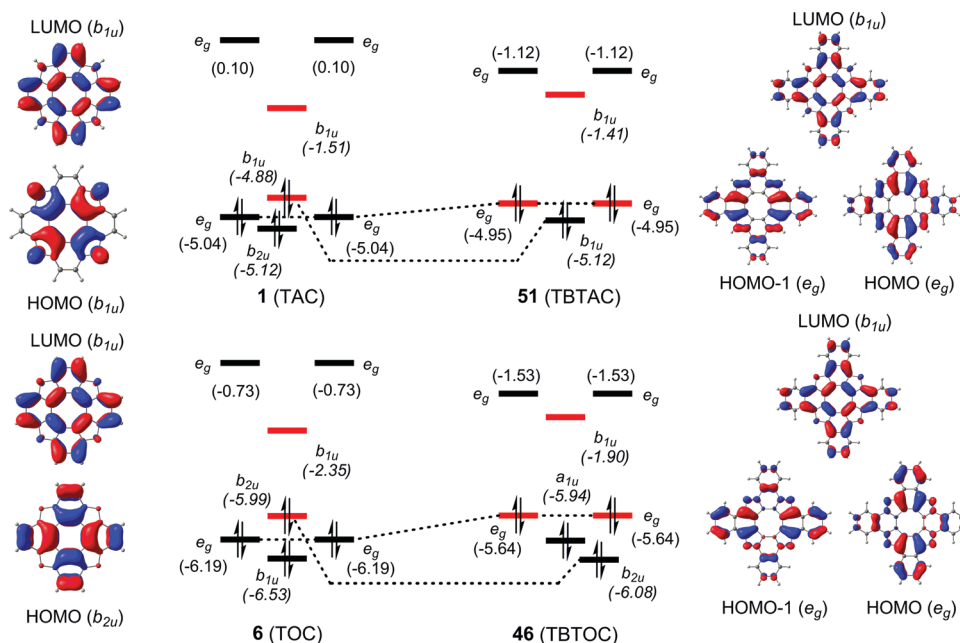


Fig. 4 The molecular orbital energy diagram for the unannellated and tetrabenzoannellated tetraaza- and tetraoxa[8]circulenes.

Table 4 Spectroscopic data for the S_0 – S_1 doubly degenerated electronic transition of TBTOC **46** and TBTAC **51**

	State ^{a,b}	$\lambda_{\text{vert}}/\lambda_{0-0}$ ^a (nm)	λ^b (nm)	f^a	f^b	λ_{exp} (nm)	Assignment ^{a,b}
46	$S_1(\times 2)$	376/405	385	0.276	0.61	411	HOMO → LUMO (1^1E_u) HOMO–1 → LUMO (2^1E_u)
	$S_1(\times 2)$	399/415	417	0.219	0.48	414	HOMO → LUMO (1^1E_u) HOMO–1 → LUMO (2^1E_u)

^a Calculations at the TDDFT/B3LYP/6-311G(d,p) level. ^b Calculations at the XMC-QDPT2/6-311(d,p) level. The S_1 state is doubly degenerate ($\times 2$).

$f_{S_0-S_1}(\mathbf{46}) > f_{S_0-S_1}(\mathbf{51})$, which are in good agreement with the experimental data (Table 4).

3.4. The vibronic spectra of TBTAC and TBTOC

In this section we present the results of the TDDFT calculations of the vibronic absorption spectra of TBTOC (**46**) and TBTAC (**51**). Accounting for the fact that the $S_0 \rightarrow S_1$ transition for both HCs was allowed, only the Franck–Condon (FC) approximation can be applied to consider the vibronic structure of this transition and the Herzberg–Teller term can be neglected. As one can see from Fig. 5, the calculated absorption spectra of both TBTAC and TBTOC consist of the main most intense 0–0 band (adiabatic transition) and well-resolved 0–1 and 0–2 vibronic satellites. However, the origin of this vibronic band was different for the isoelectronic TBTAC and TBTOC parent molecules. The 0–1 band in the spectrum of TBTOC **46** was induced mainly of the singlet excitation of ν_{139} promotive mode at 1498 cm^{-1} (Table 5), which corresponds to the bending vibrations of the CH groups together with the Kekule-type stretching vibrations of the inner benzene rings fused with the furane fragments (Fig. 6). The 0–1 band was also slightly broadened due to the excitation of the close-lying modes, 963 (0.16), 1188 (0.04), 1275 (0.08), 1326 (0.07), 1475 (0.09), 1575

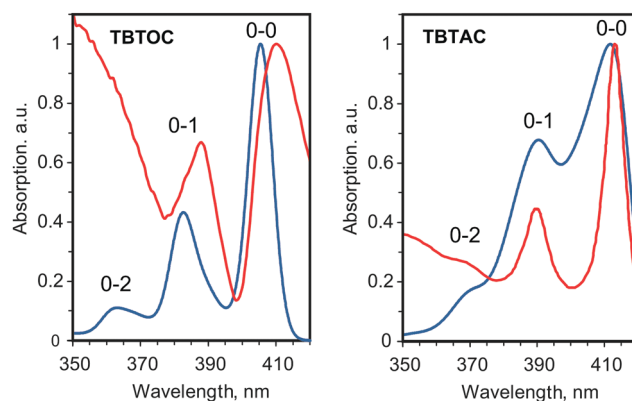


Fig. 5 The electronic absorption spectra of TBTOC and TBTAC (red lines – experimental curves, blue lines – calculated by the TDDFT/B3LYP/6-311G(d,p) method). Notably, the experimental curve for the TBTAC circulene has been taken from ref. 27 while the TBTOC experimental spectrum has been measured in this work for the first time.

(0.04), 1624 (0.08) and 1672 cm^{-1} (0.07). Herein, the Huang–Rhys factors (HRF) are presented in the parentheses as a measure of the vibrational transition probabilities; the shapes of these modes are presented in the ESI.† The 0–2 band in the spectrum

Table 5 Spectroscopic data for the 0–1 and 0–2 vibronic satellites of the S_0 – S_1 electronic transition in the absorption spectra of TBTOC **46** and TBTAC **51**

	$\lambda_{\text{calc}}/\lambda_{\text{exp}}$ (nm)	Mode	ν (cm^{-1})	HRF	Mode assignment ^a
0–1 band					
46	383/388	ν_{139}	1488	0.30	$\nu(\text{CC})_{\text{benz}}^{\text{Kekule}} + \delta(\text{CH})$
51	390/390	ν_{156}	1602	10^{-4}	$\nu(\text{CC})_{\text{benz}} + \delta(\text{CH}) + \delta(\text{NH})$
0–2 band					
46	363/—	$\nu_{139} (\times 2)$	1488 ($\times 2$)	7×10^{-3}	$\nu(\text{CC})_{\text{benz}}^{\text{Kekule}} + \delta(\text{CH})$
51	369/370	$\nu_{131} + \nu_{156}$	1376 + 1602	6×10^{-5}	$\nu_{135}; \delta(\text{NH})$ in phase + $\delta(\text{CH})$ $\nu_{160}; \nu(\text{CC})_{\text{benz}} + \delta(\text{CH}) + \delta(\text{NH})$

^a ν – stretching vibrations, δ – bending in-plane vibrations.

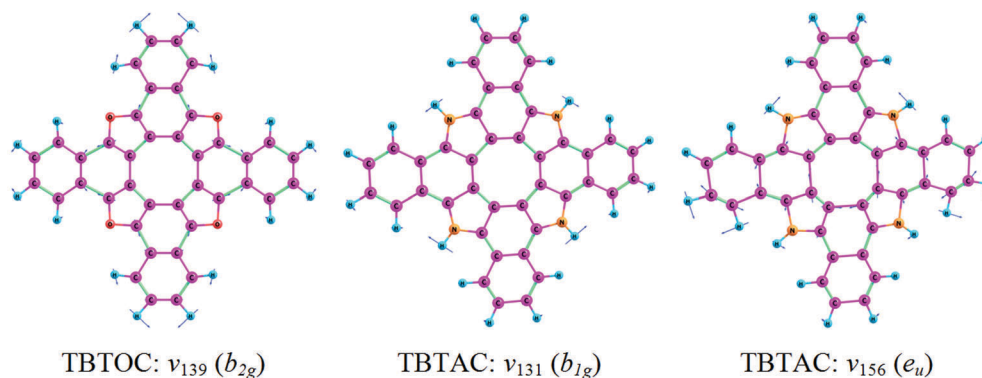


Fig. 6 The displacement vectors for the FC active modes, which produce the vibronic progression of the $S_0 \rightarrow S_1$ electronic transition in the absorption spectrum of TBTOC **46** and TBTAC **51**.

of TBTOC **46** corresponds purely to the double excitation of the ν_{139} mode (1498×2) cm^{-1} .

In the contrast to TBTOC **46**, the 0–1 band in the spectrum of TBTAC **51** corresponds to the ν_{156} mode at 1602 cm^{-1} , which combines the C=C bond stretching vibrations with the CH and NH bending vibrations (Table 5). An additional contribution to this band provides the ν_{131} mode 1375 cm^{-1} with almost the same probability as the ν_{156} mode (Table 5). Notably, the ν_{131} vibrational mode is of the pure bending type and corresponds predominantly to the in-phase bending of the four NH groups with a slight contribution from the CH in-plane bending vibrations (Fig. 6). The 0–2 band in the spectrum of TBTAC **51** (Fig. 5) corresponds to a simultaneous excitation of both ν_{131} and ν_{156} vibrational modes. Therefore, the main specificity of the TBTAC **51** vibronic absorption spectra corresponds to the fact that the bending vibrations of the NH groups are the main contributions to the promotive modes responsible for the 0–1 and 0–2 vibronic satellites. This is a clear manifestation of how the structural differences between the TBTOC **46** and TBTAC **51** molecules affect the different origins of the vibronic bands in their absorption spectra.

As can be seen from Fig. 5, the calculated and experimental vibronic absorption spectra are in agreement with respect to the band frequency and band intensity ratios except the 0–2 satellite. In the experimental spectrum of TBTAC the 0–2 transition was only barely visible in the form a broad shoulder with a maximum at 370 nm (Fig. 5 and Table 5), while in the experimental spectrum of TBTOC the 0–2 band

cannot be detected due to the increasing structureless absorption in this region.

3.5. The aromaticity of neutral and doubly charged TBTAC and TBTOC

The aromaticity of the numerous non-annelated HCs has been discussed in a number of recent publications using various aromaticity criteria such as magnetic (gauge including magnetically induced current (GIMIC) method, nuclear-independent chemical shifts (NICSS) and ^1H NMR chemical shifts), energetic (isodesmic reactions) and structural (bond alternation) parameters. In this section we have discussed how annelation and NH/O-substitution affects the aromaticity of the HCs by applying the most universal (in our opinion) GIMIC method to the neutral and doubly charged TBTAC and TBTOC molecules. As one can see from Table 6, annelation and NH/O-substitution does not affect the net character of the studied species; all the neutral HCs **1**, **6**, **46** and **51** are almost non-aromatic (the net current is close to zero), dications are anti-aromatic (the net current is paratropic) and dianions are aromatic (the net current is diatropic). Moreover, annelation and NH/O-substitution almost does not affect the net value of the magnetically induced current for the neutral and dianionic species, while the dications are very sensitive to these factors. Particularly, the dicationic tetraaza[8]circulene **1**²⁺ possesses only a small net paratropic current (-3.0 nA T^{-1}), while its tetrabenzoannelated analogue **51**²⁺ was strongly anti-aromatic with a net current of -47.5 nA T^{-1} due to the principally different origin of the current pathways in both the **1**²⁺ and

Table 6 The total ring current strength (in nA T⁻¹) and the balance between the diatropic (d) and paratropic (p) currents in the *rim*- and *hub*-subsystems for the neutral and doubly charged circulenes **1**, **6**, **46** and **51**

Species	Current ^a		Balance	Total current strength (nA T ⁻¹)	Conclusion	Source
	<i>rim</i> -system	<i>hub</i> -system				
1	d	p	d ≈ p	-0.5	Almost non-aromatic	Ref. 52
1 ²⁺	d	p	p > d	-3	Weakly anti-aromatic	Ref. 52
1 ²⁻	d	d	2d	21	Aromatic	Ref. 52
51	d	p	d ≈ p	-0.4	Almost non-aromatic	This work
51 ²⁺	p	d	p > d	-47.5	Strongly anti-aromatic	This work
51 ²⁻	d	d	2d	24	Aromatic	This work
6	d	p	p > d	-2.1	Almost non-aromatic	Ref. 52
6 ²⁺	p	d	p > d	-55	Strongly anti-aromatic	Ref. 52
6 ²⁻	d	d	2d	22	Aromatic	Ref. 52
46	d	p	d ≈ p	-0.5	Almost non-aromatic	This work
46 ²⁺	p	p	2p	-11.5	Anti-aromatic	This work
46 ²⁻	d	d	2d	26.2	Aromatic	This work

^a The current pathways distribution and current density plots can be found in the ESI.

51²⁺ species. **1**²⁺ possesses a paratropic current in the *hub*-core, which prevails slightly over the diatropic current in the *rim*-system (p > d, Table 6) whereas for the **51**²⁺ ion the *hub*-system is diatropic and the *rim*-perimeter was strongly paratropic. As a result, the **51**²⁺ cation is characterized by a strong domination of the outer paratropic current over the inner-core diatropic one (in contrast to **1**²⁺).

The dicationic tetraoxa[8]circulenes **6**²⁺ and **46**²⁺ are both anti-aromatic but their current pathways are very different. Upon benzoannulation, the inner cyclooctatetraene (COT) core of **46**²⁺ becomes strongly paratropic instead of the only slightly paratropic COT core of the **6**²⁺ ion. At the same time the strong paratropic current in the *rim*-system of the **6**²⁺ ion is decreased in the case of **46**²⁺. Thus, the non-annelated dicationic tetraoxa[8]circulene is an anti-aromatic species in contrast to the tetrabenzoannelated analogue in terms of the concept of net magnetically induced currents.

It should be noted that the current pathway calculations for the studied neutral and doubly charged circulenes **46** and **51** are in a good agreement with the NICS indices⁵² estimated using the B3LYP/6-311++G(d,p) method (Fig. S5, ESI[†]).³²⁻³⁴

Particularly, the neutral and dianionic HCs possess significantly negative NICS(0) and NICS(1) values for the benzene and furan rings indicating the presence of diatropic magnetically-induced ring currents in their *rim*-system (in complete agreement with Table 6). As for the dicationic **46**²⁺ and **51**²⁺ species they are characterized by the significantly positive NICS(0) and NICS(1) indices obtained for the benzene and furan rings in agreement with Table 6, which denotes the paratropic ring currents in the *rim*-system of dications. The NICS indices for the inner COT core are also in a good agreement with GIMIC calculations except for the **51**²⁺ ion for which NICS(0) and NICS(1) indices are positive (*i.e.* paratropic current prevails) while the GIMIC method predicts a diatropic current in the *hub*-system.

4. Experimental section

4.1. Photophysical measurements

All experiments were conducted using a 10 mm quartz cuvette and all solvents were of spectroscopic grade. The absorbance

spectrum of TBTOC (**46**) in THF was measured on a Cary 5E UV-Vis-NIR spectrophotometer. The emission spectra were measured on a Perkin Elmer LS 50 B luminescence spectrometer. Its fluorescence quantum yield was determined using a previously described protocol with 9,10-diphenylanthracene in degassed cyclohexane as the fluorescence standard.⁵³

5. Conclusions

In the present work we have for the first time presented a strategy to design new blue fluorophores on the basis of hetero-annelated tetraphenylene frameworks. We have proposed the combination of two principles – NH/O substitution and benzoannulation – to improve the emission of the non-fluorescent tetraoxa[8]circulene and azaoxa[8]circulene species. As a result we have designed 49 different fluorophores including the already synthesized tetrabenzotetraoxa[8]circulene **46** and tetrabenzo-tetraaza[8]circulene **51**, the spectral and electronic properties of which have been discussed in detail including the results obtained from quantum-chemical simulations of the vibronic absorption spectra and aromaticity features. Particularly, we have noted the different origin of the vibronic absorption bands for both compounds **45** and **51** as well as the different electronic structures and aromaticity of their doubly charged forms due to the effect of NH/O substitution. The main result of this work was the prediction of new promising mixed azaoxa[8]circulenes with very high fluorescence quantum yield values (about 0.9 and higher). Among them we should especially note the circulenes **15**, **18**, **23**, **25**, **33**, **36** and **49** with the best predicted fluorescence characteristics. We have clearly observed that the *para*-orientation of the two externally fused benzene fragments strongly enhances the fluorescence efficiency. This is due to the strong increase in the transition dipole moments for the S₀ ↔ S₁ transition being parallel to the long molecular axis, which is oriented across the opposite naphthalene fragments. The calculated φ_n values are in complete agreement with the experimental data obtained for a number of the already synthesized circulenes. Thus, we believe that the most promising circulenes designed in this work can demonstrate intense fluorescence in

the case of their successful synthesis, which in turn could be extremely useful for the fabrication of future blue OLEDs.

The role of annelation in the enhancement of the fluorescence intensity is supported by an analysis of magnetically induced currents, both aspects being determined by strong π -conjugation in the designed species.

Acknowledgements

The calculations were performed with the computational resources provided by the Swedish National Infrastructure for Computing (SNIC) at the Parallel Computer Center (PDC) through the project "Multiphysics Modeling of Molecular Materials" SNIC 020/11-23. This research was also supported by the Ministry of Education and Science of Ukraine (project number 0115U000637).

References

- G. V. Baryshnikov, B. F. Minaev and V. A. Minaeva, *Russ. Chem. Rev.*, 2015, **84**, 455.
- T. Hensel, N. N. Andersen, M. Plesner and M. Pittelkow, *Synlett*, 2016, 498.
- C. B. Nielsen, T. Brock-Nannestad, T. K. Reenberg, P. Hammershøj, J. B. Christensen, J. W. Stouwdam and M. Pittelkow, *Chem. – Eur. J.*, 2010, **16**, 13030.
- T. Fujimoto, M. M. Matsushita and K. Awaga, *J. Phys. Chem. C*, 2012, **116**, 5240.
- T. Fujimoto, M. M. Matsushita and K. Awaga, *Appl. Phys. Lett.*, 2010, **97**, 123303.
- A. Dadvand, F. Cicoira, K. Yu. Chernichenko, E. S. Balenkova, R. M. Osuna, F. Rosei, V. G. Nenajdenko and D. F. Perepichka, *Chem. Commun.*, 2008, 5354.
- G. Baryshnikov, B. Minaev, N. Karaush and V. Minaeva, *Phys. Chem. Chem. Phys.*, 2014, **16**, 6555.
- G. Baryshnikov, B. Minaev, N. Karaush and V. Minaeva, *RSC Adv.*, 2014, **4**, 25843.
- J. Yu, Q. Sun, Y. Kawazoe and P. Jena, *Nanoscale*, 2014, **6**, 14962.
- N. N. Karaush, G. V. Baryshnikov and B. F. Minaev, *RSC Adv.*, 2015, **5**, 24299.
- N. N. Karaush, G. V. Baryshnikov, B. A. Minaeva and B. F. Minaev, *New J. Chem.*, 2015, **39**, 7815.
- L.-W. Shi, B. Chen, J.-H. Zhou, T. Zhang, Q. Kang and M.-B. Chen, *J. Phys. Chem. A*, 2008, **112**, 11724.
- T. N. Gribanova, N. S. Zefirov and V. I. Minkin, *Pure Appl. Chem.*, 2010, **82**, 1011.
- G. V. Baryshnikov, R. R. Valiev, N. N. Karaush and B. F. Minaev, *Phys. Chem. Chem. Phys.*, 2014, **16**, 15367.
- G. V. Baryshnikov, N. N. Karaush, R. R. Valiev and B. F. Minaev, *J. Mol. Model.*, 2015, **21**, 136.
- S. Radenković, I. Gutman and P. Bultinck, *J. Phys. Chem. A*, 2012, **116**, 9421.
- G. V. Baryshnikov, B. F. Minaev, M. Pittelkow, C. B. Nielsen and R. Salcedo, *J. Mol. Model.*, 2013, **19**, 847.
- G. V. Baryshnikov, R. R. Valiev, N. N. Karaush, D. Sundholm and B. F. Minaev, *Phys. Chem. Chem. Phys.*, 2016, **18**, 8980.
- H. Erdtman and H.-E. Högberg, *Chem. Commun.*, 1968, 773.
- H. Erdtman and H.-E. Högberg, *Tetrahedron Lett.*, 1970, **11**, 3389.
- K. Yu. Chernichenko, V. V. Sumerin, R. V. Shpanchenko, E. S. Balenkova and V. G. Nenajdenko, *Angew. Chem., Int. Ed.*, 2006, **45**, 7367.
- C. B. Nielsen, T. Brock-Nannestad, P. Hammershøj, T. K. Reenberg, M. Schau-Magnussen, D. Trpceviski, T. Hensel, R. Salcedo, G. V. Baryshnikov, B. F. Minaev and M. Pittelkow, *Chem. – Eur. J.*, 2013, **19**, 3898.
- T. Hensel, D. Trpceviski, C. Lind, R. Grosjean, P. Hammershøj, C. B. Nielsen, T. Brock-Nannestad, B. E. Nielsen, M. Schau-Magnussen, B. Minaev, G. V. Baryshnikov and M. Pittelkow, *Chem. – Eur. J.*, 2013, **19**, 17097.
- M. Plesner, T. Hensel, B. E. Nielsen, F. S. Kamounah, T. Brock-Nannestad, C. B. Nielsen, C. G. Tortzen, O. Hammerich and M. Pittelkow, *Org. Biomol. Chem.*, 2015, **13**, 5937.
- X. Xiong, C.-L. Deng, B. F. Minaev, G. V. Baryshnikov, X.-S. Peng and H. N. C. Wong, *Chem. – Asian J.*, 2015, **10**, 969.
- G. V. Baryshnikov, V. A. Minaeva, B. F. Minaev, N. N. Karaush, X.-D. Xiong, M.-D. Li, D. L. Phillips and H. N. C. Wong, *Spectrochim. Acta, Part A*, 2015, **151**, 247.
- F. Chen, Y. S. Hong, S. Shimizu, D. Kim, T. Tanaka and A. Osuka, *Angew. Chem., Int. Ed.*, 2015, **54**, 10639.
- B. F. Minaev, G. V. Baryshnikov and V. A. Minaeva, *Comput. Theor. Chem.*, 2011, **972**, 68.
- N. N. Karaush, B. F. Minaev, G. V. Baryshnikov and V. A. Minaeva, *Opt. Spectrosc.*, 2014, **116**, 33.
- J. Yin, K. Chaitanya and X.-H. Ju, *J. Mater. Chem. C*, 2015, **3**, 3472.
- X.-D. Tang, Y. Liao, H.-Z. Gao, Y. Geng and Z.-M. Su, *J. Mater. Chem.*, 2012, **22**, 6907.
- A. D. Becke, *J. Chem. Phys.*, 1993, **98**, 5648.
- C. Lee, W. Yang and R. G. Parr, *Phys. Rev. B: Condens. Matter Mater. Phys.*, 1988, **37**, 785.
- K. Raghavachari, J. S. Binkley, R. Seeger and J. A. Pople, *J. Chem. Phys.*, 1980, **72**, 650.
- M. J. Frisch, G. W. Trucks, H. B. Schlegel, G. E. Scuseria, M. A. Robb, J. R. Cheeseman, G. Scalmani, V. Barone, B. Mennucci, G. A. Petersson, H. Nakatsuji, M. Caricato, X. Li, H. P. Hratchian, A. F. Izmaylov, J. Bloino, G. Zheng, J. L. Sonnenberg, M. Hada, M. Ehara, K. Toyota, R. Fukuda, J. Hasegawa, M. Ishida, T. Nakajima, Y. Honda, O. Kitao, H. Nakai, T. Vreven, J. A. Montgomery, Jr., J. E. Peralta, F. Ogliaro, M. Bearpark, J. J. Heyd, E. Brothers, K. N. Kudin, V. N. Staroverov, R. Kobayashi, J. Normand, K. Raghavachari, A. Rendell, J. C. Burant, S. S. Iyengar, J. Tomasi, M. Cossi, N. Rega, J. M. Millam, M. Klene, J. E. Knox, J. B. Cross, V. Bakken, C. Adamo, J. Jaramillo, R. Gomperts, R. E. Stratmann, O. Yazyev, A. J. Austin, R. Cammi, C. Pomelli, J. W. Ochterski, R. L. Martin, K. Morokuma, V. G. Zakrzewski, G. A. Voth, P. Salvador, J. J. Dannenberg, S. Dapprich, A. D. Daniels, O. Farkas, J. B. Foresman, J. V. Ortiz,

- J. Cioslowski, D. J. Fox, *Gaussian 09. Rev. D.01*, Gaussian Inc., Wallingford, CT, 2013.
- 36 E. Runge and E. K. U. Gross, *Phys. Rev. Lett.*, 1984, **52**, 997.
- 37 S. Miertuš, E. Scrocco and J. Tomasi, *Chem. Phys.*, 1981, **55**, 117.
- 38 A. A. Granovsky, *J. Chem. Phys.*, 2011, **134**, 214113.
- 39 J. Finley, P.-Å. Malmqvist, B. O. Roos and L. Serrano-Andrés, *Chem. Phys. Lett.*, 1998, **288**, 299.
- 40 A. A. Granovsky, Firefly version 8.0.0, <http://classic.chem.msu.su/gran/firefly/index.html>.
- 41 (a) R. R. Valiev, V. N. Cherepanov, V. Ya. Artyukhov and D. Sundholm, *Phys. Chem. Chem. Phys.*, 2012, **14**, 11508; (b) V. Ya. Artyukhov and A. I. Galeeva, *Russ. Phys. J.*, 1986, **29**, 949.
- 42 (a) V. G. Plotnikov, *Int. J. Quantum Chem.*, 1979, **16**, 527; (b) S. Knuts, B. F. Minaev, H. Ågren and O. Vahtras, *Theor. Chim. Acta*, 1994, **87**, 343; (c) B. F. Minaev, *Fizika Molekul*, 1979, **7**, 34; (d) G. V. Maier, V. Ya. Artyukhov and N. R. Rib, *Russ. Phys. J.*, 1993, **36**, 949; (e) V. Y. Artyukhov, A. I. Galeeva, G. V. Maier and V. V. Ponomarev, *Opt. Spektrosk.*, 1997, **82**, 520; (f) V. Ya. Artyukhov and V. A. Pomogaev, *Russ. Phys. J.*, 2000, **43**, 590; (g) V. A. Pomogaev and V. Ya. Artyukhov, *J. Appl. Spectrosc.*, 2001, **68**, 251.
- 43 H. Fliegl, S. Taubert, O. Lehtonen and D. Sundholm, *Phys. Chem. Chem. Phys.*, 2011, **13**, 20500.
- 44 J. Jusélius, D. Sundholm and J. Gauss, *J. Chem. Phys.*, 2004, **121**, 3952.
- 45 H. Fliegl, D. Sundholm, S. Taubert, J. Jusélius and W. Klopper, *J. Phys. Chem. A*, 2009, **113**, 8668.
- 46 H. Fliegl, N. Özcan, R. Mera-Adasme, F. Pichierri, J. Jusélius and D. Sundholm, *Mol. Phys.*, 2013, **111**, 1364.
- 47 R. R. Valiev and V. N. Cherepanov, *Int. J. Quantum Chem.*, 2013, **113**, 2563.
- 48 R. R. Valiev, H. Fliegl and D. Sundholm, *Phys. Chem. Chem. Phys.*, 2014, **16**, 11010.
- 49 F. Furche, R. Ahlrichs, C. Hättig, W. Klopper, M. Sierkam and F. Weigend, *Comput. Mol. Sci.*, 2014, **4**, 91.
- 50 JMOL: an open-source Java viewer for chemical structures in 3D, <http://www.jmol.org>.
- 51 N. N. Karaush, R. R. Valiev, G. V. Baryshnikov, B. F. Minaev and H. Ågren, *Chem. Phys.*, 2015, **459**, 65.
- 52 Z. Chen, C. S. Wannere, C. Corminboeuf, R. Puchta and P. v. R. Schleyer, *Chem. Rev.*, 2005, **105**, 3842.
- 53 C. Würth, M. Grabolle, J. Pauli, M. Spieles and U. Resch-genger, *Nat. Protoc.*, 2013, **8**, 1535.